ACS APPLIED MATERIALS & INTERFACES

www.acsami.org

Research Article

Electron Irradiation of Metal Contacts in Monolayer MoS_2 Field-Effect Transistors

Aniello Pelella, Osamah Kharsah, Alessandro Grillo, Francesca Urban, Maurizio Passacantando, Filippo Giubileo, Laura Iemmo, Stephan Sleziona, Erik Pollmann, Lukas Madauß, Marika Schleberger, and Antonio Di Bartolomeo*

Cite This: https://dx.doi.org/10.1021/acsami.0c11933

Read Online

ACCESS | Metrics & More | Article Recommendations

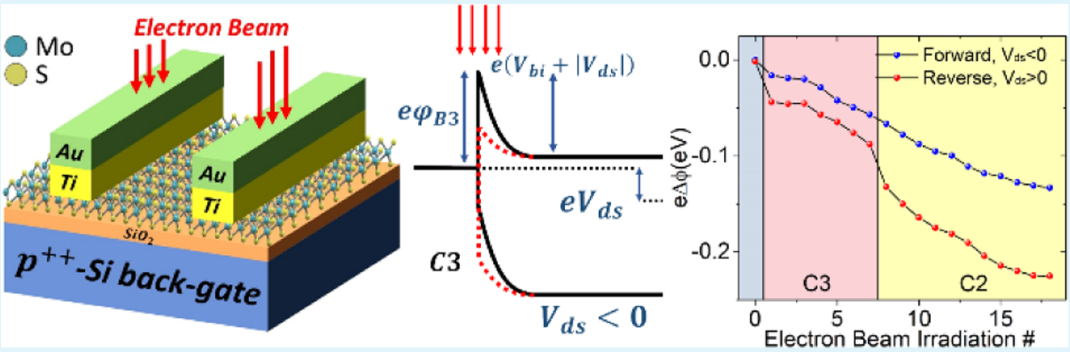

ABSTRACT: Metal contacts play a fundamental role in nanoscale devices. In this work, Schottky metal contacts in monolayer molybdenum disulfide (MoS_2) field-effect transistors are investigated under electron beam irradiation. It is shown that the exposure of Ti/Au source/drain electrodes to an electron beam reduces the contact resistance and improves the transistor performance. The electron beam conditioning of contacts is permanent, while the irradiation of the channel can produce transient effects. It is demonstrated that irradiation lowers the Schottky barrier at the contacts because of thermally induced atom diffusion and interfacial reactions. The simulation of electron paths in the device reveals that most of the beam energy is absorbed in the metal contacts. The study demonstrates that electron beam irradiation can be effectively used for contact improvement though local annealing.

KEYWORDS: *molybdenum disulfide, field-effect transistors, Schottky barrier, scanning electron microscopy, Raman spectroscopy, photoluminescence, electron beam irradiation, electron interactions in solids*

INTRODUCTION

Molybdenum disulfide (MoS_2) is one of the most studied transition metal dichalcogenides, owing to its layered structure and useful mechanical, chemical, electronic, and optoelectronic properties.[1−4] A molybdenum (Mo) atomic plane sandwiched between two sulfur (S) planes constitutes the monolayer that is bonded to other monolayers by weak van der Waals forces to form the bulk material. MoS_2 is a semiconductor suitable for several applications,[5−9] having a 1.2 eV indirect band gap in the bulk form that widens up to 1.8−1.9 eV and becomes direct in the monolayer.[3] Despite the lower field-effect mobility than graphene,[10,11] ranging from few tenths to hundreds[12−15] of cm^2 V^{-1} s^{-1}, MoS_2 field-effect transistors (FETs) have recently become very popular as alternatives to graphene FETs[12−17] for next-generation electronics based on 2D materials.[18−25]

The fabrication and characterization of devices based on 2D materials greatly rely on the application of electron beam (e-beam) lithography or focused ion beam processing and on scanning electron microscopy (SEM) or transmission electron microscopy, which imply irradiation by charged particles. The exposure to low-energy electrons and/or ions can modify the electronic properties of the 2D materials or their interfaces.[9,17,26] Indeed, structural defects can locally modify the band structure and behave as charge traps, thereby changing the device characteristics both in the case of e-beam[27,28] and ion beam irradiation.[29,30] Conversely, electron beam, ion irradiation, or plasma treatments can be intentionally used for nanoincisions,[31] for pores,[32] or to purposely create defects, for instance, to reduce the contact resistance.[33−35] Choi et al.

Received: July 1, 2020
Accepted: August 10, 2020
Published: August 10, 2020

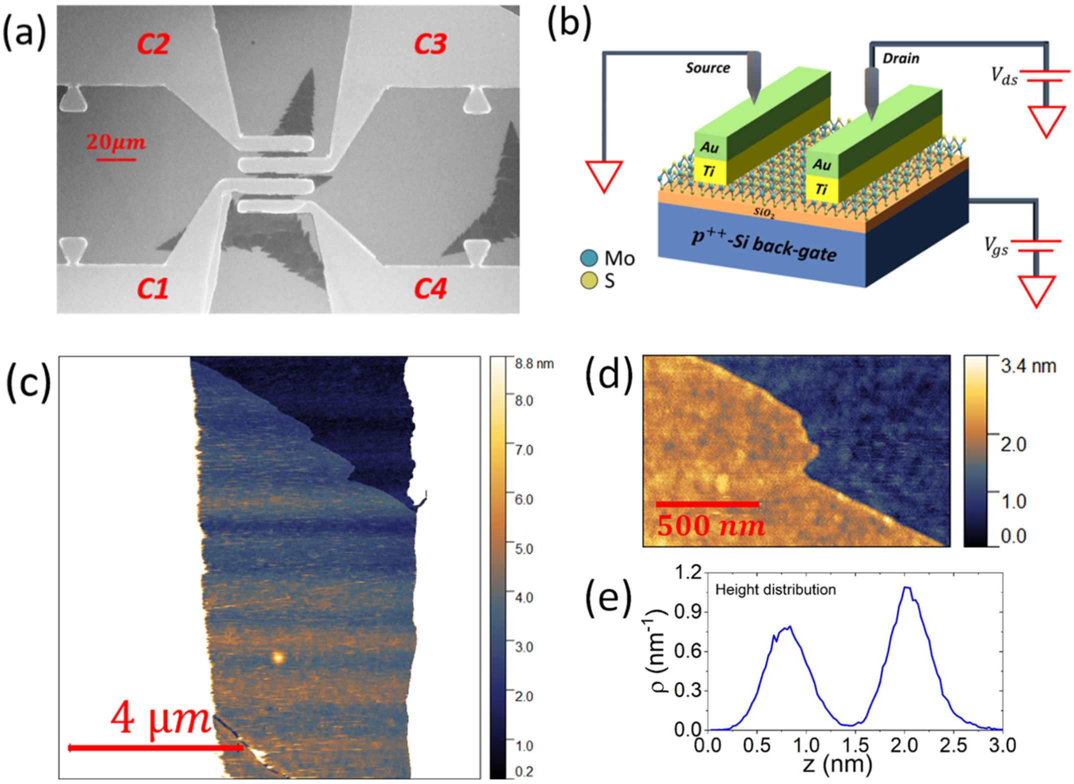

Figure 1. (a) SEM image of the MoS_2 device and contact labels. (b) MoS_2 FET layout and schematic of the common source configuration used for electrical characterization. (c) AFM image of the MoS_2 flake between the electrical contacts, which appear here in white as the scale has been adjusted to properly image the MoS_2 flake. (d) Zoom-in into the upper region of (c), showing that the flake is flat and structurally intact. The rms roughness is 0.221 nm for the SiO_2 substrate and 0.237 nm for MoS_2. (e) Height distribution taken from image (d), yielding a height of ∼1.2 nm.

reported the effects of 30 keV electron beam irradiation of monolayer MoS_2 FETs, showing that irradiation-induced defects act as trap sites by reducing the carrier mobility and concentration and shifting the threshold voltage.[36] A study of point defects in MoS_2 using SEM imaging and first-principles calculations, by Zhou et al., demonstrated that vacancies are created by e-beam irradiation at low energies,[37] below 30 keV. Durand et al. studied the effects of e-beam on the MoS_2-based FET, reporting an increase in carrier density and a decrease in mobility explained as irradiation-induced generation of intrinsic defects in MoS_2 and as Coulomb scattering by charges at the MoS_2−SiO_2 interface, respectively.[38] Giubileo et al. reported a negative threshold voltage shift and a carrier mobility enhancement under 10 keV electron irradiation of few-layer MoS_2 FETs attributed to beam-induced positive charge trapped in the SiO_2 gate oxide.

In this paper, we present the spectroscopic and electrical characterization of monolayer MoS_2-based FETs, with Schottky Ti/Au contacts, focusing on the effects of low-energy e-beam irradiation. We show that the long exposure of the metal contacts to 10 keV e-beam in a SEM chamber enhances the transistor's on-current. We explain such an improvement by radiation-induced lowering of the Schottky barrier at the metal contacts. We perform Monte Carlo simulation to track the e-beam through the device and show that when the beam is focused onto the contacts, most of the beam energy is absorbed within the metal. The local heat can induce atomic diffusion and interfacial reactions that change the chemical composition and structure of the metal−MoS_2 interface or can generate or release tensile strain. Both effects cause the lowering of the Schottky barrier and the consequent increase in transistor current.

Our study shows that electron beam exposure during SEM imaging has non-negligible effects on MoS_2 devices; however, it also highlights that a suitable exposure, with the e-beam focused on the contact region, can be conveniently exploited to reduce the contact resistance of the transistor. Compared to thermal annealing, our finding provides a way to improve the contact resistance by local conditioning, which avoids the exposure of the entire wafer to a high thermal budget.

■ FABRICATION AND EXPERIMENTAL METHODS

The MoS_2 monolayer flakes were grown via chemical vapor deposition in a three-zone split tube furnace, purged with 1000 N cm^3/min Ar gas for 15 min to minimize the O_2 content. The growth SiO_2/Si substrate was spin-coated with a 1% sodium cholate solution; then, a saturated ammonium heptamolybdate (AHM) solution was first annealed at 300 °C under ambient conditions to turn AHM into MoO_3 to be used as the source for molybdenum. The target material was placed in a three-zone tube furnace along with 50 mg of S powder, positioned upstream in a separate heating zone. The zones containing S and AHM were heated to 150 °C and 750 °C, respectively. After 15 min of growth, the process was stopped, and the sample was cooled rapidly.

We realized FETs using the SiO_2/Si substrate (thickness of the dielectric: 285 nm) as the back gate and evaporating the drain and source electrodes on selected MoS_2 flakes through standard photolithography and lift-off processes. The contacts were made of Ti (10 nm) and Au (40 nm) used as adhesion and cover layers, respectively. Ti was deposited in high vacuum, which could not exclude the formation of TiO_2, contributing to the resistance and Schottky barrier at the contacts. Figure 1a,b shows the SEM top view of a typical device and its schematic layout and measurement setup.

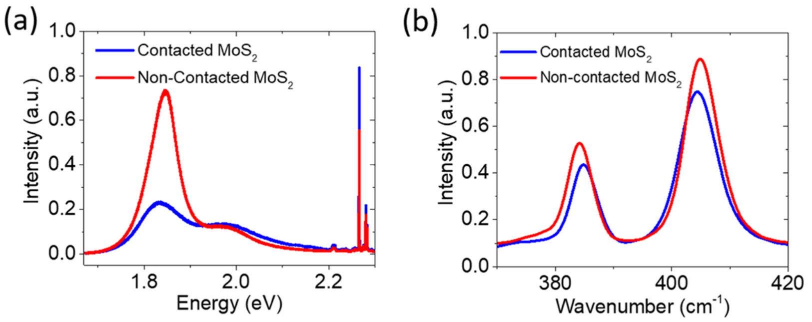

Figure 2. (a) PL and (b) Raman spectrum of monolayer MoS_2 after FET processing. Blue: contacted MoS_2 monolayer flake and red: noncontacted monolayer MoS_2 flake.

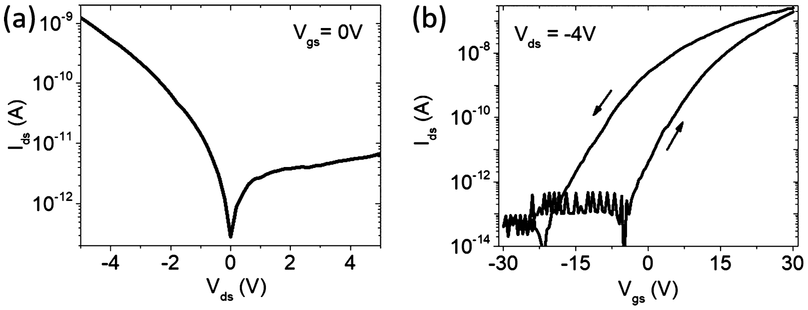

Figure 3. Output (a) and transfer (b) characteristics of the device between C2 and C3 contacts, with C3 used as the drain and C2 as the grounded source.

The channel is made up from a monolayer flake [as confirmed by Raman and photoluminescence (PL), see below] of width and length of 20 and 4 μm, respectively, and a nominal thickness of 0.7 nm. Atomic force microscope (AFM) images (Figure 1c,d) show that the flake has an average height of 1.0−1.3 nm (which is typical for single-layer MoS_2 measured in air by AFM) and appears to be extremely flat (roughness rms < 0.25 nm) and structurally intact. There are some contaminants because of the lithography process, which are weakly bound and can be swept by the AFM tip. Contacted and noncontacted flake areas do not differ with respect to contamination density—spectroscopic data should thus be comparable.

A total of seven MoS_2 channels of identically prepared FETs have been characterized by Raman and PL spectroscopy just after processing. The measurements were performed with a Renishaw InVia Raman microscope at the Interdisciplinary Center for Analytics on the Nanoscale (ICAN). The excitation laser wavelength was 532 nm, and the power density was kept below 0.1 mW/μm^2 to avoid damage to the MoS_2 flake. Exemplary spectra of Raman characterization are shown in Figure 2. The chosen reference measurements are spectra obtained from MoS_2 flakes on the same substrate, which were also in contact with the photoresist and various solvents during the processing and lift-off for the production of the FETs, but are not in contact with metal electrodes themselves. The shape of the PL spectra (Figure 2a) and the difference of the Raman modes (Figure 2b) differ significantly. The PL intensity (sum of all excitons and trions) for noncontacted MoS_2 flakes is higher by a factor of 1.7 ± 0.8 than that for contacted MoS_2. The mode differences for noncontacted and contacted MoS_2 are 21.3 ± 0.7 cm^{-1} and 19.7 ± 0.7 cm^{-1}, respectively. Both the changes in PL and Raman mode difference can be associated with built-in strain or changes in the electronic properties and the band structure of the MoS_2 sheets.[39−43] From the linear dependencies of Raman mode positions on doping and strain,[39,40] we find a reduction of tensile strain by (0.46 ± 0.28) % and an increase in electron doping of $0.44 \pm 0.36 \times 10^{13}$ electrons per cm^2 for the contacted 2D material in comparison with noncontacted MoS_2 (details of the calculation method can be found in ref 44). Hence, the significant alterations in the spectroscopic precharacterization of the MoS_2 channels can be clearly attributed to electronic and structural changes at the metal contact.

In the following, most of the electrical characterization refers to the transistor between the contacts labeled C2 and C3 in Figure 1a. The contact C3 was used as the drain and C2 as the grounded source. The electrical measurements were carried out inside a SEM chamber (LEO 1530, Zeiss), endowed with two metallic probes with nanometer positioning capability, connected to a Keithley 4200 SCS (source measurement units, Tektronix Inc.), at room temperature and a pressure of about 10^{-6} mbar. The e-beam of SEM, set to 10 keV and 10 pA, was used for the time-controlled irradiation of specific parts of the device.

■ RESULTS AND DISCUSSION

The output ($I_{ds}-V_{ds}$) and the transfer ($I_{ds}-V_{gs}$) characteristics of the transistor are shown in Figure 3a,b, respectively. The output curve shows rectification with the forward current appearing at negative V_{ds}, typical of a p-type Schottky diode, while the transfer characteristic shows an n-type transistor. This apparently contradictory behavior has been previously reported for MoS_2 and WSe_2 transistors and explained by the formation of two back-to-back and possibly asymmetric Schottky barriers at the contacts.[45,46] The forward current at negative V_{ds} is caused by the different contact areas and by the image force barrier lowering of the forced junction (i.e., the drain, C3, in our case), while the reverse current at $V_{ds} > 0$ V is limited by the grounded junction at the source (C2) contact. As the barrier lowering is more effective on the forced junction, the voltage being directly applied to it, the negative bias gives rise to the higher (apparently forward) current.

After the initial electrical characterization, we performed two sets of exposures to the SEM electron beam. Each exposure lasted 300 s, corresponding to a fluence of ∼180 e^-/nm^2, over a surface of ∼100 μm^2. The two sets of irradiations were carried out first on the drain contact (C3) and then on the

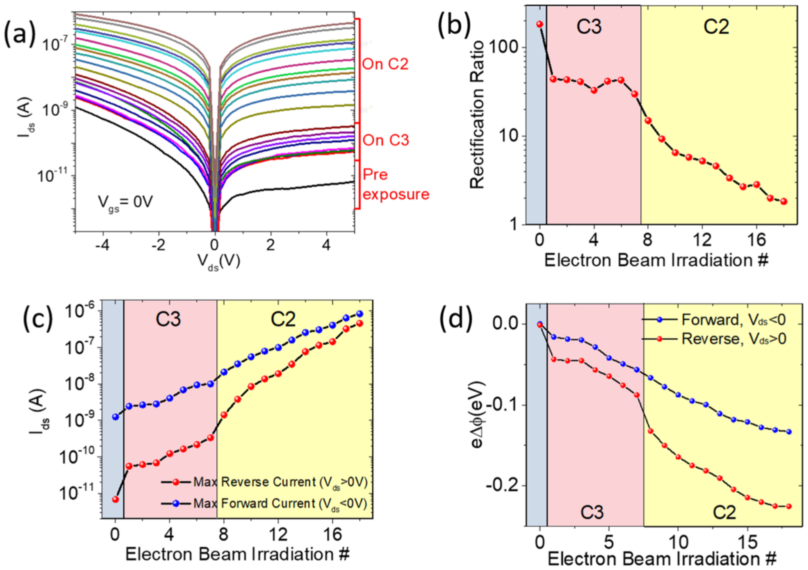

Figure 4. (a) Output characteristics at V_{gs} = 0 V of the transistor formed by contacts C2−C3 exposed to two sets of electron irradiations performed first on contact C3 and then on C2. (b) Rectification ratio and (c) maximum forward and reverse current, at V_{ds} = ±5 V, as a function of the irradiation number. (d) Zero-bias Schottky barrier variation at the contacts C2 and C3 as a function of the irradiation number.

grounded source contact (C2). A final exposure of the MoS_2 channel to the e-beam was performed as well.

Figure 4 summarizes the obtained results. The $I_{ds}-V_{ds}$ curves were measured at the end of each irradiation, ∼120 s after the blanking of the e-beam, to allow cooling down. Starting from the bottom (black) line in Figure 4a, representing the output curve of the unexposed device, the current increases with the e-beam exposures. We note two major discontinuities in the sequence of $I_{ds}-V_{ds}$ curves, corresponding to the start of the two irradiations sets. These gaps are likely due to the uncontrolled exposure of the whole device during the selection of the drain (C3) and grounded source (C2) contact areas for the respective irradiation sets.

A different behavior of the forward with respect to the reverse current can be observed in Figure 4a, and a distinction of the effects of the irradiations on the drain (C3) and the grounded source (C2) can be made. Although the irradiation of the drain increases both the forward and the reverse currents, keeping the rectification ratio almost constant (see Figure 4 b), the irradiation of the source augments the reverse current in a faster way, rendering the output curves more symmetric. Figure 4b shows that repeated irradiations of the drain contact (C3) do not change the rectification ratio (at V_{ds} = ±5 V), while the irradiation of the grounded source contact (C2) dramatically decreases the rectification ratio. Figure 4c shows that the maximum reverse and forward currents, at V_{ds} = ±5 V, have different variation rates when the irradiation is either on the drain or source. Noticeably, Figure 4c shows that the increase in both the reverse and forward currents is an exponential function of the fluence, which is proportional to and can be parametrized by the irradiation number.

As the shape and the current intensity of the output characteristics are related to the Schottky barrier heights at the contacts, the exponentially increasing current and the changing rectification ratio point to radiation-induced Schottky barrier lowering. The energy release in the metal contacts can modify the chemistry of the metal−MoS_2 interface or create stress and defects that can lead to a lowering of the barrier and a consequent contact resistance reduction. We note that the reduction of contact resistance by chemical reactions between the metal contacts and MoS_2 channel has been reported for the metal deposited under ultrahigh vacuum[47] and contact laser annealing.[48] A disordered, compositionally graded layer, composed of Mo and Ti_xS_y species, forms on the surface of the MoS_2 crystal following the deposition of Ti, and thermal annealing in the 100−600 °C temperature range can cause Ti diffusion inducing further chemical and structural changes at the Ti−MoS_2 interface.[49,50] It is also possible that diffusion of Au atoms to the interface with MoS_2 occurs under the energetic electron beam irradiation. Au does not react with MoS_2 but reduces the contact resistance and therefore the Schottky barrier height.[51]

Similarly, tensile strain has been demonstrated to induce considerable Schottky and tunneling barrier lowering.[52]

A Schottky barrier of ∼0.2 eV is formed by several metals on MoS_2 because of Fermi level pinning below the MoS_2 conduction band.[53−55] Density functional theory calculations have indicated that the pinning at the metal−MoS_2 interface is different from the well-known Bardeen pinning effect, metal-induced gap states, and defect/disorder-induced gap states, which are applicable to traditional metal−semiconductor junctions. At metal−MoS_2 interfaces, the Fermi level is pinned either by a metal work function modification due to interface dipole formation arising from the charge redistribution or by the production of gap states mainly of Mo d-orbitals, characterized by the weakened intralayer S−Mo bonding because of the interface metal−S interaction.[56,57] The observed decrease in the Schottky barrier by e-beam irradiation, up to its complete disappearance, supports the occurrence of interface modifications that cause Fermi level depinning.

As the forward current at V_{ds} < 0 V is limited by the Schottky barrier at the drain contact (C3), while the reverse current at V_{ds} > 0 V is limited by the Schottky barrier at the grounded source contact C2 (which are the reverse-biased junctions for negative and positive V_{ds}, respectively), the output curves of Figure 4a, which correspond always to reverse current, can be used to extract the behavior of the Schottky barriers as a function of the fluence (i.e., the e-beam irradiation

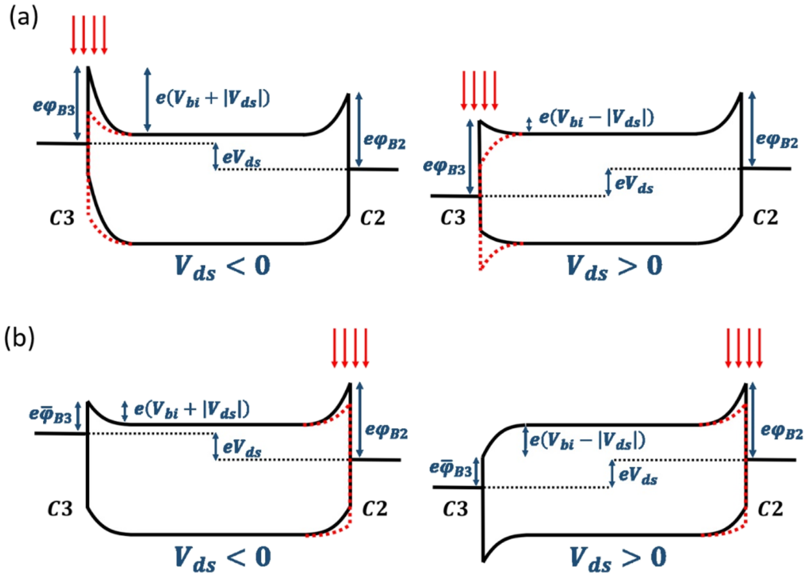

Figure 5. Low-bias energy band diagrams (black) and their modification under electron irradiation (red) of C3 (a) and of C2 (b) contacts resulting in barrier lowering ($\overline{\varphi}_B$).

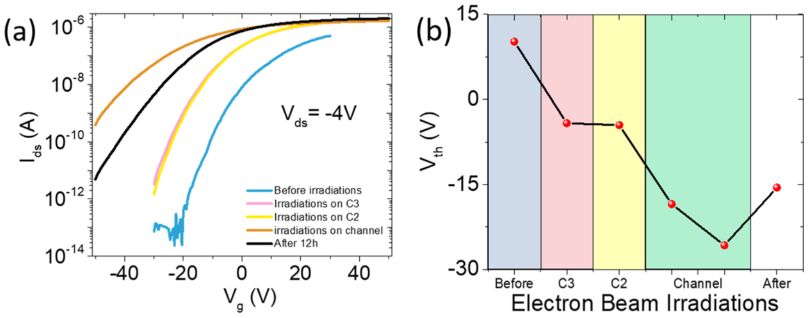

Figure 6. (a) FET transfer characteristics at V_{ds} = −4 V before and after e-beam irradiations of contacts C3 and C2 and of the channel. (b) Left shift of the threshold voltage extrapolated from the transfer characteristics over the e-beam exposure.

number). Let us consider the thermionic current through a reverse-biased Schottky barrier[58,59]

$$I_n = I_{sn}[e^{eV_a/nkT} - 1] = [SA^*_{2D}T^{3/2}e^{-e\varphi_{Bn}/kT}][e^{eV_a/nkT} - 1] \approx -SA^*_{2D}T^{3/2}e^{-e\varphi_{Bn}/kT} \qquad (1)$$

where φ_{Bn} and I_{sn} are the barrier height and the reverse saturation current at the n-th e-beam irradiation, S is the junction area, A^*_{2D} is the 2D Richardson constant, k is the Boltzmann constant, T is the temperature, n is the ideality factor, and V_a is the negative voltage across the barrier that makes $e^{eV_a/nkT} \approx 0$. Let us define I_o as the reverse saturation current before e-beam exposure, that is, associated to the maximum barrier height φ_{B0}. To avoid the effect of bias which can induce image-force barrier lowering,[60] both I_n and I_0 are obtained by extrapolating the measured currents to zero bias. Then, eq 1 can be used to evaluate the variation of the Schottky barrier, $\Delta\varphi_{Bn} = \varphi_{Bn} - \varphi_{B0}$, as a function of the irradiation number

$$\ln\left(\frac{I_n}{I_0}\right) = -\frac{e\Delta\varphi_{Bn}}{kT} \rightarrow \Delta\varphi_{Bn} = -\frac{kT}{e}\ln\left(\frac{I_n}{I_0}\right) \qquad (2)$$

The zero-bias Schottky barrier variation, $\Delta\varphi_{Bn}$, is shown in Figure 4d for both source (C2) and drain (C3) contacts. The overall reduction of both barriers is comparable to the expected initial barrier height based on Fermi level pinning, meaning that the long irradiation can completely remove the barriers. The plot indicates that the two barriers behave differently for the irradiation of C2 or C3. Although the beam irradiation of either contact results in a lowering of both Schottky barriers, the barrier decrease is faster for the irradiation of the grounded source. Besides, the Schottky barrier at the source contact is the most affected by the irradiation of the source.

To explain these results, we propose the model based on the energy band diagrams, shown in Figure 5. A negative (positive) voltage applied to the drain contact (C3) causes an upward (downward) shift of the energy bands in the drain region. Electron beam irradiation of the contact lowers the Schottky barrier and the relative built-in potential, as shown by the red dashed lines in Figure 5. The reduction of a Schottky barrier and of its associated built-in potential, at the irradiated contact, results also in the lowering of the unexposed barrier, which can experience a stronger potential drop because of the reduced contact resistance of the first contact. Figure 5a represents the situation in which the e-beam is focused on the biased drain contact (C3). At $V_{ds} < 0$ V, the current is limited mainly by the drain contact barrier which is lowered by the successive irradiations, causing the exponential increase in maximum forward current. At $V_{ds} > 0$ V, the current is limited by the un-

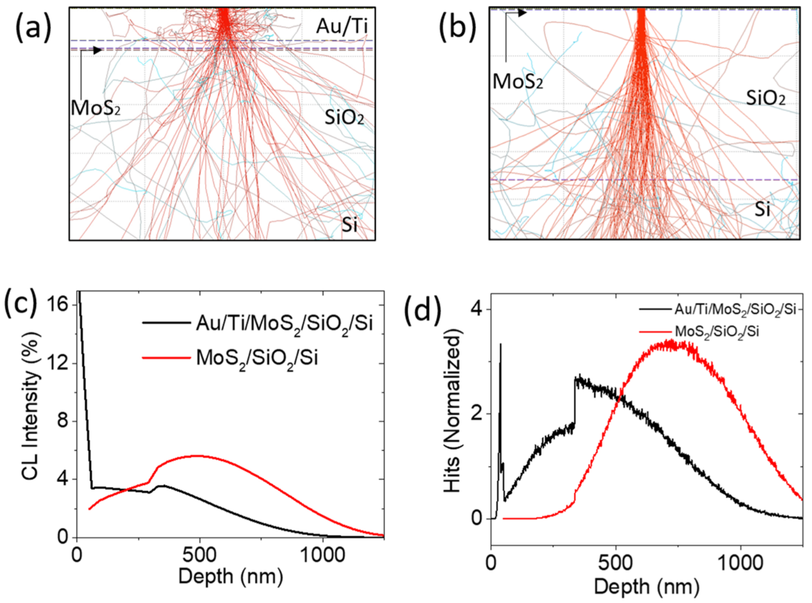

Figure 7. Monte Carlo simulation using CASINO v2 of e-beam irradiation of the device (a) contacts and (b) of the MoS_2 channel. (c) Simulated cathodoluminescence intensity through the sample, with the e-beam focused onto contacts and onto the flake. (d) Simulation of the electron's penetration depth through the sample.

irradiated source contact (C2) barrier, and its dependence on the irradiation cycle is caused by the lowering of the built-in potential at the drain (C3). As the barrier and built-in lowering are the same, the rectification ratio remains almost constant. For irradiation of the grounded source (C2, Figure 5b), the current increases because of a similar mechanism, with the difference that the drain contact barrier limits the current for $V_{ds} > 0$ V to a lesser extent, having been already irradiation-lowered. Therefore, the reverse current increases faster with the repeated irradiation and the rectification ratio decreases.

The effect of irradiation on the transfer characteristic of the transistor is shown in Figure 6 and confirms the radiation-induced increase in channel current. Besides, Figure 6a shows that the e-beam, independent of onto which contact it is focused on, causes a left shift of the transfer curve. Such a shift corresponds to a decrease in threshold voltage, defined as the x-axis intercept of the linear fit of the transfer curve on the linear scale. The threshold voltage as a function of the irradiation is displayed in Figure 6b. Although the e-beam exposure of the contacts provokes a left shift (the transfer curves are taken at the end of the two irradiation sets on the drain (C3) and grounded source (C2)), further left shift of the threshold voltage is observed when two successive irradiations are performed in the channel region.

The observed negative shift of the threshold voltage has been reported and discussed before.[27] It can be explained by the pile-up of positive charge in trap states of the SiO_2 gate dielectric or at the SiO_2−Si interface. The e-beam exposures produce electron−hole pairs in the SiO_2 gate oxide and in the Si substrate: although mobile electrons are easily swept by the applied bias, the positive charges can be stored for long times.[27] The positive charge storage acts as an extra gate (similarly to the gating effect under light irradiation[61,62]) and enhances the n-type doping of the channel.

Indeed, Figure 6 shows that there is a slight recovery of the threshold voltage after 12 h of annealing at room temperature. However, we highlight that, as demonstrated by Figure 6a, the maximum channel current, which is limited by the contact resistances, remains unchanged after annealing, demonstrating that the irradiation-induced improvement of the contacts is permanent.

To further confirm our model, we performed a Monte Carlo simulation to track the path of the electrons under the contacts and in the channel region (Figure 7a,b), using the CASINO software package.[63−65] We simulated a 10 keV beam with one million electrons and a radius beam of 10 nm. The cathodoluminescence spectrum (Figure 7c) shows that electrons lose their energy and are stopped (Figure 7d) mostly in the Ti/Au metal stack, while they reach and are absorbed in the Si substrate when the irradiation is on the channel. The high release of energy in the metal contacts, similarly to thermal annealing,[66,67] induces Ti−MoS_2 reactions and creates contact with the reduced Schottky barrier and contact resistance. Conversely, when we directly irradiate the MoS_2 channel, energy is prevalently adsorbed in the Si bulk and its effect manifests only through the positive charge traps generated in the SiO_2 layer.

CONCLUSIONS

We investigated the effects of 10 keV electron beam irradiation of the Schottky metal contacts in MoS_2-based FETs. Spectroscopic analysis by Raman and PL shows that the presence of metal contacts changes the properties of monolayer MoS_2 with respect to strain and doping. The electrical measurements revealed that electron beam irradiation improves the device conductance, reduces the rectification of the output characteristic, and causes a left shift of the threshold voltage. To explain such a feature, we propose that the energy absorbed in the metal contacts induces atomic diffusion and interfacial reactions that lower the Schottky barrier at the contacts and improve the contact resistance. We corroborate our model by direct measurement of the Schottky barrier height variation and by simulation of the electron trajectories in the contact regions.

AUTHOR INFORMATION

Corresponding Author

Antonio Di Bartolomeo − *Department of Physics and Interdepartmental Centre NanoMates, University of Salerno, Fisciano 84084, Italy; CNR-SPIN, Fisciano 84084, Italy;* orcid.org/0000-0002-3629-726X; Email: adibartolomeo@unisa.it

Authors

Aniello Pelella − *Department of Physics and Interdepartmental Centre NanoMates, University of Salerno, Fisciano 84084, Italy; CNR-SPIN, Fisciano 84084, Italy;* orcid.org/0000-0002-3831-0210

Osamah Kharsah − *Fakultät für Physik and CENIDE, Universität Duisburg-Essen, Duisburg 47057, Germany*

Alessandro Grillo − *Department of Physics and Interdepartmental Centre NanoMates, University of Salerno, Fisciano 84084, Italy; CNR-SPIN, Fisciano 84084, Italy;* orcid.org/0000-0002-8909-9865

Francesca Urban − *Department of Physics and Interdepartmental Centre NanoMates, University of Salerno, Fisciano 84084, Italy; CNR-SPIN, Fisciano 84084, Italy; INFN—Gruppo Collegato di Salerno, Fisciano 84084, Italy;* orcid.org/0000-0003-2109-1370

Maurizio Passacantando − *Department of Physical and Chemical Sciences, University of L'Aquila, and CNR-SPIN L'Aquila, L'Aquila 67100, Italy;* orcid.org/0000-0002-3680-5295

Filippo Giubileo − *CNR-SPIN, Fisciano 84084, Italy;* orcid.org/0000-0003-2233-3810

Laura Iemmo − *Department of Physics and Interdepartmental Centre NanoMates, University of Salerno, Fisciano 84084, Italy; CNR-SPIN, Fisciano 84084, Italy*

Stephan Sleziona − *Fakultät für Physik and CENIDE, Universität Duisburg-Essen, Duisburg 47057, Germany*

Erik Pollmann − *Fakultät für Physik and CENIDE, Universität Duisburg-Essen, Duisburg 47057, Germany;* orcid.org/0000-0002-3961-0426

Lukas Madauß − *Fakultät für Physik and CENIDE, Universität Duisburg-Essen, Duisburg 47057, Germany;* orcid.org/0000-0003-2556-5967

Marika Schleberger − *Fakultät für Physik and CENIDE, Universität Duisburg-Essen, Duisburg 47057, Germany;* orcid.org/0000-0002-5785-1186

Complete contact information is available at:
https://pubs.acs.org/10.1021/acsami.0c11933

Notes

The authors declare no competing financial interest.

ACKNOWLEDGMENTS

A.D.B. acknowledges the financial support from MIUR—Italian Ministry of Education, University and Research (projects Pico & Pro ARS01_01061 and RINASCIMENTO ARS01_01088). M.S. acknowledges the financial support from DFG—German Research Foundation (project number 406129719). The authors thank ICAN—facility founded by the German Research Foundation (DFG, reference RI_00313)—for Raman and PL spectroscopy.

REFERENCES

(1) Santhosh, S.; Madhavan, A. A. A Review on the Structure, Properties and Characterization of 2D Molybdenum Disulfide. *In 2019 Advances in Science and Engineering Technology International Conferences (ASET)*; IEEE: Dubai, United Arab Emirates, 2019; pp 1−5.

(2) Urban, F.; Passacantando, M.; Giubileo, F.; Iemmo, L.; Di Bartolomeo, A. Transport and Field Emission Properties of MoS2 Bilayers. *Nanomaterials* **2018**, *8*, 151.

(3) Mak, K. F.; Lee, C.; Hone, J.; Shan, J.; Heinz, T. F. Atomically Thin MoS2 : A New Direct-Gap Semiconductor. *Phys. Rev. Lett.* **2010**, *105*, 136805.

(4) Urban, F.; Giubileo, F.; Grillo, A.; Iemmo, L.; Luongo, G.; Passacantando, M.; Foller, T.; Madauß, L.; Pollmann, E.; Geller, M. P.; Oing, D.; Schleberger, M.; Di Bartolomeo, A. Gas Dependent Hysteresis in MoS_2 Field Effect Transistors. *2D Mater.* **2019**, *6*, 045049.

(5) Hasani, A.; Le, Q. V.; Tekalgne, M.; Choi, M.-J.; Lee, T. H.; Jang, H. W.; Kim, S. Y. Direct Synthesis of Two-Dimensional MoS2 on p-Type Si and Application to Solar Hydrogen Production. *NPG Asia Mater.* **2019**, *11*, 47.

(6) Bazaka, K.; Levchenko, I.; Lim, J. W. M.; Baranov, O.; Corbella, C.; Xu, S.; Keidar, M. MoS_2 -Based Nanostructures: Synthesis and Applications in Medicine. *J. Phys. D: Appl. Phys.* **2019**, *52*, 183001.

(7) Giubileo, F.; Grillo, A.; Passacantando, M.; Urban, F.; Iemmo, L.; Luongo, G.; Pelella, A.; Loveridge, M.; Lozzi, L.; Di Bartolomeo, A. Field Emission Characterization of MoS2 Nanoflowers. *Nanomaterials* **2019**, *9*, 717.

(8) Dragoman, M.; Cismaru, A.; Aldrigo, M.; Radoi, A.; Dinescu, A.; Dragoman, D. MoS $_2$ Thin Films as Electrically Tunable Materials for Microwave Applications. *Appl. Phys. Lett.* **2015**, *107*, 243109.

(9) Madauß, L.; Zegkinoglou, I.; Vázquez Muiños, H.; Choi, Y.-W.; Kunze, S.; Zhao, M.-Q.; Naylor, C. H.; Ernst, P.; Pollmann, E.; Ochedowski, O.; Lebius, H.; Benyagoub, A.; Ban-d'Etat, B.; Johnson, A. T. C.; Djurabekova, F.; Roldan Cuenya, B.; Schleberger, M. Highly Active Single-Layer MoS_2 Catalysts Synthesized by Swift Heavy Ion Irradiation. *Nanoscale* **2018**, *10*, 22908−22916.

(10) Urban, F.; Lupina, G.; Grillo, A.; Martucciello, N.; Di Bartolomeo, A. Contact Resistance and Mobility in Back-Gate Graphene Transistors. *Nano Express* **2020**, *1*, 010001.

(11) Bolotin, K. I. Electronic Transport in Graphene: Towards High Mobility. *Graphene*; Elsevier, 2014; pp 199−227.

(12) Di Bartolomeo, A.; Santandrea, S.; Giubileo, F.; Romeo, F.; Petrosino, M.; Citro, R.; Barbara, P.; Lupina, G.; Schroeder, T.; Rubino, A. Effect of Back-Gate on Contact Resistance and on Channel Conductance in Graphene-Based Field-Effect Transistors. *Diamond Relat. Mater.* **2013**, *38*, 19−23.

(13) Wilmart, Q.; Boukhicha, M.; Graef, H.; Mele, D.; Palomo, J.; Rosticher, M.; Taniguchi, T.; Watanabe, K.; Bouchiat, V.; Baudin, E.; Berroir, J.-M.; Bocquillon, E.; Fève, G.; Pallecchi, E.; Plaçais, B. High-Frequency Limits of Graphene Field-Effect Transistors with Velocity Saturation. *Appl. Sci.* **2020**, *10*, 446.

(14) Piccinini, E.; Alberti, S.; Longo, G. S.; Berninger, T.; Breu, J.; Dostalek, J.; Azzaroni, O.; Knoll, W. Pushing the Boundaries of Interfacial Sensitivity in Graphene FET Sensors: Polyelectrolyte Multilayers Strongly Increase the Debye Screening Length. *J. Phys. Chem. C* **2018**, *122*, 10181−10188.

(15) Di Bartolomeo, A.; Giubileo, F.; Iemmo, L.; Romeo, F.; Russo, S.; Unal, S.; Passacantando, M.; Grossi, V.; Cucolo, A. M. Leakage and Field Emission in Side-Gate Graphene Field Effect Transistors. *Appl. Phys. Lett.* **2016**, *109*, 023510.

(16) Bartolomeo, A. D.; Giubileo, F.; Romeo, F.; Sabatino, P.; Carapella, G.; Iemmo, L.; Schroeder, T.; Lupina, G. Graphene Field Effect Transistors with Niobium Contacts and Asymmetric Transfer Characteristics. *Nanotechnology* **2015**, *26*, 475202.

(17) Li, F.; Gao, F.; Xu, M.; Liu, X.; Zhang, X.; Wu, H.; Qi, J. Tuning Transport and Photoelectric Performance of Monolayer MoS $_2$ Device by E-Beam Irradiation. *Adv. Mater. Interfaces* **2018**, *5*, 1800348.

(18) Wang, J.; Yao, Q.; Huang, C.-W.; Zou, X.; Liao, L.; Chen, S.; Fan, Z.; Zhang, K.; Wu, W.; Xiao, X.; Jiang, C.; Wu, W.-W. High Mobility MoS$_2$ Transistor with Low Schottky Barrier Contact by Using Atomic Thick h-BN as a Tunneling Layer. *Adv. Mater.* **2016**, *28*, 8302−8308.

(19) Fiori, G.; Bonaccorso, F.; Iannaccone, G.; Palacios, T.; Neumaier, D.; Seabaugh, A.; Banerjee, S. K.; Colombo, L. Electronics Based on Two-Dimensional Materials. *Nat. Nanotechnol.* **2014**, *9*, 768−779.

(20) Kim, M. J.; Choi, Y.; Seok, J.; Lee, S.; Kim, Y. J.; Lee, J. Y.; Cho, J. H. Defect-Free Copolymer Gate Dielectrics for Gating MoS$_2$ Transistors. *J. Phys. Chem. C* **2018**, *122*, 12193−12199.

(21) Rasmussen, F. A.; Thygesen, K. S. Computational 2D Materials Database: Electronic Structure of Transition-Metal Dichalcogenides and Oxides. *J. Phys. Chem. C* **2015**, *119*, 13169−13183.

(22) Di Bartolomeo, A.; Pelella, A.; Liu, X.; Miao, F.; Passacantando, M.; Giubileo, F.; Grillo, A.; Iemmo, L.; Urban, F.; Liang, S. J. Pressure-Tunable Ambipolar Conduction and Hysteresis in Thin Palladium Diselenide Field Effect Transistors. *Adv. Funct. Mater.* **2019**, *29*, 1902483.

(23) Di Bartolomeo, A.; Luongo, G.; Iemmo, L.; Urban, F.; Giubileo, F. Graphene−Silicon Schottky Diodes for Photodetection. *IEEE Trans. Nanotechnol.* **2018**, *17*, 1133−1137.

(24) Jin, C.; Rasmussen, F. A.; Thygesen, K. S. Tuning the Schottky Barrier at the Graphene/MoS$_2$ Interface by Electron Doping: Density Functional Theory and Many-Body Calculations. *J. Phys. Chem. C* **2015**, *119*, 19928−19933.

(25) Grillo, A.; Di Bartolomeo, A.; Urban, F.; Passacantando, M.; Caridad, J. M.; Sun, J.; Camilli, L. Observation of 2D Conduction in Ultrathin Germanium Arsenide Field-Effect Transistors. *ACS Appl. Mater. Interfaces* **2020**, *12*, 12998−13004.

(26) Schleberger, M.; Kotakoski, J. 2D Material Science: Defect Engineering by Particle Irradiation. *Materials* **2018**, *11*, 1885.

(27) Giubileo, F.; Iemmo, L.; Passacantando, M.; Urban, F.; Luongo, G.; Sun, L.; Amato, G.; Enrico, E.; Di Bartolomeo, A. Effect of Electron Irradiation on the Transport and Field Emission Properties of Few-Layer MoS$_2$ Field-Effect Transistors. *J. Phys. Chem. C* **2019**, *123*, 1454−1461.

(28) Di Bartolomeo, A.; Urban, F.; Pelella, A.; Grillo, A.; Passacantando, M.; Liu, X.; Giubileo, F. Electron Irradiation of Multilayer PdSe$_2$ Field Effect Transistors. *Nanotechnology* **2020**, *31*, 375204.

(29) Ochedowski, O.; Marinov, K.; Wilbs, G.; Keller, G.; Scheuschner, N.; Severin, D.; Bender, M.; Maultzsch, J.; Tegude, F. J.; Schleberger, M. Radiation Hardness of Graphene and MoS$_2$ Field Effect Devices against Swift Heavy Ion Irradiation. *J. Appl. Phys.* **2013**, *113*, 214306.

(30) Ernst, P.; Kozubek, R.; Madauß, L.; Sonntag, J.; Lorke, A.; Schleberger, M. Irradiation of Graphene Field Effect Transistors with Highly Charged Ions. *Nucl. Instrum. Methods Phys. Res., Sect. B* **2016**, *382*, 71−75.

(31) Madauß, L.; Ochedowski, O.; Lebius, H.; Ban-d'Etat, B.; Naylor, C. H.; Johnson, A. T. C.; Kotakoski, J.; Schleberger, M. Defect Engineering of Single- and Few-Layer MoS$_2$ by Swift Heavy Ion Irradiation. *2D Mater.* **2016**, *4*, 015034.

(32) Kozubek, R.; Tripathi, M.; Ghorbani-Asl, M.; Kretschmer, S.; Madauß, L.; Pollmann, E.; O'Brien, M.; McEvoy, N.; Ludacka, U.; Susi, T.; Duesberg, G. S.; Wilhelm, R. A.; Krasheninnikov, A. V.; Kotakoski, J.; Schleberger, M. Perforating Freestanding Molybdenum Disulfide Monolayers with Highly Charged Ions. *J. Phys. Chem. Lett.* **2019**, *10*, 904−910.

(33) Giubileo, F.; Di Bartolomeo, A. The Role of Contact Resistance in Graphene Field-Effect Devices. *Prog. Surf. Sci.* **2017**, *92*, 143−175.

(34) Shahzad, K.; Jia, K.; Zhao, C.; Wang, D.; Usman, M.; Luo, J. Effects of Different Ion Irradiation on the Contact Resistance of Pd/Graphene Contacts. *Materials* **2019**, *12*, 3928.

(35) Yan, X.; Jia, K.; Su, Y.; Ma, Y.; Luo, J.; Zhu, H.; Wei, Y. Edge-Contact Formed by Oxygen Plasma and Rapid Thermal Annealing to Improve Metal-Graphene Contact Resistance. *ECS J. Solid State Sci. Technol.* **2018**, *7*, M11−M15.

(36) Choi, B. Y.; Cho, K.; Pak, J.; Kim, T.-Y.; Kim, J.-K.; Shin, J.; Seo, J.; Chung, S.; Lee, T. Effects of Electron Beam Irradiation and Thiol Molecule Treatment on the Properties of MoS2 Field Effect Transistors. *J. Korean Phys. Soc.* **2018**, *72*, 1203−1208.

(37) Zhou, W.; Zou, X.; Najmaei, S.; Liu, Z.; Shi, Y.; Kong, J.; Lou, J.; Ajayan, P. M.; Yakobson, B. I.; Idrobo, J.-C. Intrinsic Structural Defects in Monolayer Molybdenum Disulfide. *Nano Lett.* **2013**, *13*, 2615−2622.

(38) Durand, C.; Zhang, X.; Fowlkes, J.; Najmaei, S.; Lou, J.; Li, A.-P. Defect-Mediated Transport and Electronic Irradiation Effect in Individual Domains of CVD-Grown Monolayer MoS$_2$. *J. Vac. Sci. Technol., B: Nanotechnol. Microelectron.: Mater., Process., Meas., Phenom.* **2015**, *33*, 02B110.

(39) Rice, C.; Young, R. J.; Zan, R.; Bangert, U.; Wolverson, D.; Georgiou, T.; Jalil, R.; Novoselov, K. S. Raman-Scattering Measurements and First-Principles Calculations of Strain-Induced Phonon Shifts in Monolayer MoS 2. *Phys. Rev. B: Condens. Matter Mater. Phys.* **2013**, *87*, 081307.

(40) Chakraborty, B.; Bera, A.; Muthu, D. V. S.; Bhowmick, S.; Waghmare, U. V.; Sood, A. K. Symmetry-Dependent Phonon Renormalization in Monolayer MoS2 Transistor. *Phys. Rev. B: Condens. Matter Mater. Phys.* **2012**, *85*, 161403.

(41) Scheuschner, N.; Ochedowski, O.; Kaulitz, A.-M.; Gillen, R.; Schleberger, M.; Maultzsch, J. Photoluminescence of Freestanding Single- and Few-Layer MoS2. *Phys. Rev. B: Condens. Matter Mater. Phys.* **2014**, *89*, 125406.

(42) Conley, H. J.; Wang, B.; Ziegler, J. I.; Haglund, R. F.; Pantelides, S. T.; Bolotin, K. I. Bandgap Engineering of Strained Monolayer and Bilayer MoS$_2$. *Nano Lett.* **2013**, *13*, 3626−3630.

(43) Mak, K. F.; He, K.; Lee, C.; Lee, G. H.; Hone, J.; Heinz, T. F.; Shan, J. Tightly Bound Trions in Monolayer MoS2. *Nat. Mater.* **2013**, *12*, 207−211.

(44) Pollmann, E.; Madauß, L.; Schumacher, S.; Kumar, U.; Heuvel, F.; Ende, C. vom.; Yilmaz, S.; Gündörmüs, S.; Schleberger, M. Apparent Differences between Single Layer Molybdenum Disulfide Fabricated via Chemical Vapor Deposition and Exfoliation. **2020**, arXiv:2006.05789 [cond-mat].

(45) Di Bartolomeo, A.; Grillo, A.; Urban, F.; Iemmo, L.; Giubileo, F.; Luongo, G.; Amato, G.; Croin, L.; Sun, L.; Liang, S.-J.; Ang, L. K. Asymmetric Schottky Contacts in Bilayer MoS2 Field Effect Transistors. *Adv. Funct. Mater.* **2018**, *28*, 1800657.

(46) Di Bartolomeo, A.; Urban, F.; Passacantando, M.; McEvoy, N.; Peters, L.; Iemmo, L.; Luongo, G.; Romeo, F.; Giubileo, F. A WSe2 Vertical Field Emission Transistor. *Nanoscale* **2019**, *11*, 1538−1548.

(47) Smyth, C. M.; Addou, R.; McDonnell, S.; Hinkle, C. L.; Wallace, R. M. Contact Metal−MoS$_2$ Interfacial Reactions and Potential Implications on MoS$_2$ -Based Device Performance. *J. Phys. Chem. C* **2016**, *120*, 14719−14729.

(48) Kwon, H.; Baik, S.; Jang, J.; Jang, J.; Kim, S.; Grigoropoulos, C.; Kwon, H.-J. Ultra-Short Pulsed Laser Annealing Effects on MoS2 Transistors with Asymmetric and Symmetric Contacts. *Electronics* **2019**, *8*, 222.

(49) Freedy, K. M.; Zhang, H.; Litwin, P. M.; Bendersky, L. A.; Davydov, A. V.; McDonnell, S. Thermal Stability of Titanium Contacts to MoS$_2$. *ACS Appl. Mater. Interfaces* **2019**, *11*, 35389−35393.

(50) McDonnell, S.; Smyth, C.; Hinkle, C. L.; Wallace, R. M. MoS$_2$ −Titanium Contact Interface Reactions. *ACS Appl. Mater. Interfaces* **2016**, *8*, 8289−8294.

(51) English, C. D.; Shine, G.; Dorgan, V. E.; Saraswat, K. C.; Pop, E. Improved Contacts to MoS$_2$ Transistors by Ultra-High Vacuum Metal Deposition. *Nano Lett.* **2016**, *16*, 3824−3830.

(52) Wang, Q.; Deng, B.; Shi, X. A New Insight for Ohmic Contacts to MoS$_2$: By Tuning MoS$_2$ Affinity Energies but Not Metal Work-Functions. *Phys. Chem. Chem. Phys.* **2017**, *19*, 26151−26157.

(53) Kim, C.; Moon, I.; Lee, D.; Choi, M. S.; Ahmed, F.; Nam, S.; Cho, Y.; Shin, H.-J.; Park, S.; Yoo, W. J. Fermi Level Pinning at

Electrical Metal Contacts of Monolayer Molybdenum Dichalcogenides. *ACS Nano* **2017**, *11*, 1588−1596.

(54) Guo, Y.; Liu, D.; Robertson, J. 3D Behavior of Schottky Barriers of 2D Transition-Metal Dichalcogenides. *ACS Appl. Mater. Interfaces* **2015**, *7*, 25709−25715.

(55) Pan, Y.; Gu, J.; Tang, H.; Zhang, X.; Li, J.; Shi, B.; Yang, J.; Zhang, H.; Yan, J.; Liu, S.; Hu, H.; Wu, M.; Lu, J. Reexamination of the Schottky Barrier Heights in Monolayer MoS_2 Field-Effect Transistors. *ACS Appl. Nano Mater.* **2019**, *2*, 4717−4726.

(56) Gong, C.; Colombo, L.; Wallace, R. M.; Cho, K. The Unusual Mechanism of Partial Fermi Level Pinning at Metal−MoS_2 Interfaces. *Nano Lett.* **2014**, *14*, 1714−1720.

(57) Zhong, H.; Quhe, R.; Wang, Y.; Ni, Z.; Ye, M.; Song, Z.; Pan, Y.; Yang, J.; Yang, L.; Lei, M.; Shi, J.; Lu, J. Interfacial Properties of Monolayer and Bilayer MoS2 Contacts with Metals: Beyond the Energy Band Calculations. *Sci. Rep.* **2016**, *6*, 21786.

(58) Di Bartolomeo, A. Graphene Schottky Diodes: An Experimental Review of the Rectifying Graphene/Semiconductor Heterojunction. *Phys. Rep.* **2016**, *606*, 1−58.

(59) Anwar, A.; Nabet, B.; Culp, J.; Castro, F. Effects of Electron Confinement on Thermionic Emission Current in a Modulation Doped Heterostructure. *J. Appl. Phys.* **1999**, *85*, 2663−2666.

(60) Sze, S. M.; Ng, K. K. *Physics of Semiconductor Devices*; John Wiley & Sons, Inc.: Hoboken, NJ, USA, 2006.

(61) Di Bartolomeo, A.; Genovese, L.; Foller, T.; Giubileo, F.; Luongo, G.; Croin, L.; Liang, S.-J.; Ang, L. K.; Schleberger, M. Electrical Transport and Persistent Photoconductivity in Monolayer MoS_2 Phototransistors. *Nanotechnology* **2017**, *28*, 214002.

(62) Zhang, K.; Peng, M.; Yu, A.; Fan, Y.; Zhai, J.; Wang, Z. L. A Substrate-Enhanced MoS $_2$ Photodetector through a Dual-Photogating Effect. *Mater. Horiz.* **2019**, *6*, 826−833.

(63) Cheng, Y. J.; Yan, L.; Shi, F.; Liu, F.; Li, M.; Shi, H. L.; Hou, Z. P. Monte Carlo Simulation of Electron Scattering in Ion Barrier Film in Generation III Image Intensifier. *Key Eng. Mater.* **2013**, *552*, 193−200.

(64) Movla, H.; Babazadeh, M. Simulation Analysis of the Aluminum Thin Film Thickness Measurement by Using Low Energy Electron Beam. *Optik* **2014**, *125*, 71−74.

(65) Drouin, D.; Couture, A. R.; Joly, D.; Tastet, X.; Aimez, V.; Gauvin, R. CASINO V2.42—A Fast and Easy-to-Use Modeling Tool for Scanning Electron Microscopy and Microanalysis Users. *Scanning* **2007**, *29*, 92−101.

(66) Abraham, M.; Mohney, S. E. Annealed Ag Contacts to MoS $_2$ Field-Effect Transistors. *J. Appl. Phys.* **2017**, *122*, 115306.

(67) Goyal, N.; Mackenzie, D. M. A.; Panchal, V.; Jawa, H.; Kazakova, O.; Petersen, D. H.; Lodha, S. Enhanced Thermally Aided Memory Performance Using Few-Layer ReS2 Transistors. *Appl. Phys. Lett.* **2020**, *116*, 052104.

https://dx.doi.org/10.1021/acsami.0c11933